

---

# Self-Supervised Representation Learning as Multimodal Variational Inference

---

**Hiroki Nakamura**

Panasonic Holdings Corp.

nakamura.hiroki003@jp.panasonic.com

**Masashi Okada**

Panasonic Holdings Corp.

okada.masashi001@jp.panasonic.com

**Tadahiro Taniguchi**

Ritsumeikan University

taniguchi@em.ci.ritsumei.ac.jp

## Abstract

In this paper, we propose a probabilistic extension of the recent self-supervised learning (SSL) method, SimSiam. The proposed extension makes SimSiam uncertainty-aware by considering SimSiam as a generative model of augmented views and learning it in terms of variational inference. SimSiam trains a model by maximizing the similarity between image representations of different augmented views of the same image. The augmentation process sometimes produces ambiguous images, and their representations potentially have uncertainty. Although the use of uncertainty-aware machine learning becoming common, such as in deep variational inference, SimSiam and other SSL methods are insufficiently uncertainty-aware, leading to limitations in the use of augmented ambiguous images. Our main contributions are twofold: Firstly, we clarify the theoretical relationship between non-contrastive SSL and multimodal variational inference. Secondly, we introduce a novel SSL called variational inference SimSiam (VI-SimSiam), which incorporates uncertainty by involving spherical posterior distributions. The experiment results show that VI-SimSiam outperforms SimSiam in classification tasks in several datasets, such as ImageNette and ImageWoof by successfully estimating the representation uncertainty.

## 1 Introduction

Self-supervised learning (SSL) is a framework for learning representations of data, e.g., images without labels [4, 11, 15, 5, 3, 50, 41, 29, 22, 31]. Non-contrastive SSL such as SimSiam [4] and BYOL [11] is one of the state-of-the-art methods, which trains image encoders by maximizing the similarity between representations of different augmented views of the same image. Given that this method uses many images by random augmentations, some image representations potentially have uncertainty. However, the SSL methods have not explicitly modeled the uncertainty, suppressing learning performance because of similarity mismatch caused by uncertain representations.

Probabilistic generative models with variational inference is another approach for representation learning [21], which learns latent representations in an unsupervised fashion by training inference and generative models (i.e., autoencoders) together. This can naturally incorporate uncertainty in representations by predicting the latent distribution parameters like variance, given that the variational inference is probabilistically derived. However, in generative representation learning methods, the pixel-wise objective for reconstruction is sensitive to rare samples [25]. Furthermore, this type of representation learning was recently found to be less competitive than SSL methods on the benchmarking classification tasks [25, 29]. Incorporating the probabilistic concepts of variational

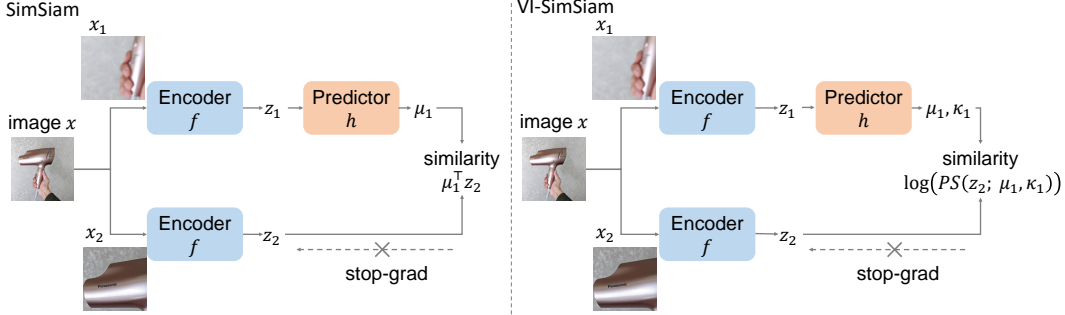


**Figure 1:** Overview of the comparison between our method and SimSiam [4]. These methods use augmented images  $x_1$  and  $x_2$  as input images. SimSiam cannot model the uncertainty of image representations. Therefore, image representations with high uncertainty cause similarity mismatch, thus suppress learning. On the other hand, VI-SimSiam predicts an image representation that follows the Power Spherical distribution [8]. VI-SimSiam can model the uncertainty of image representations and reduce the harmful effect of uncertain image representations on learning.

inference into SSL methods seems promising to make the SSL models uncertainty-aware. Although SSL and variational inference seem highly related in the view of learning representations without supervision, their theoretical connection has not been fully explored.

In this paper, we incorporate the concept of variational inference and make SSL uncertainty-aware. The contributions of this study are summarized as follows.

- We clarify the theoretical relationship between non-contrastive SSL (i.e., SimSiam and BYOL) and variational inference, which generalizes SSL methods as multimodal variational inference of spherical latent variables.
- We derive a novel non-contrastive SSL method from the theoretical relationship, which called variational inference SimSiam (VI-SimSiam). The result of the linear evaluation shows that VI-SimSiam outperforms SimSiam on the classification tasks on several datasets, such as ImageNette and ImageWoof.

We illustrate a comparison of SimSiam and VI-SimSiam in Fig. 1, where VI-SimSiam estimates the uncertainty by predicting latent distributions.

## 2 Related work

### 2.1 Non-Contrastive Self-supervised learning

Non-contrastive SSL (e.g., SimSiam [4] and BYOL [11]) methods have demonstrated to have notable performance on many downstream tasks, such as classification and object detection. Unlike contrastive SSL methods [3, 15], non-contrastive SSL methods learn a model using only different augmented views of the same image (positive pairs). Tian et al. [41] conducted a theoretical analysis on why the non-contrastive methods work well. Zbontar et al. [50] proposed another type of non-contrastive method using the redundancy-reduction principle of neuroscience. However, the above-mentioned studies did not consider uncertainty on the latent variable.

### 2.2 Variational inference

Variational inference in deep learning is generally formulated using auto-encoding variational Bayes [21]. The variational inference estimate latent distributions such as Gaussian [21], Gaussian mixture [42], and von Mises-Fischer (vMF) distribution for *spherical* random variables [7]. Although Wang et al. [44] pointed out that SSL methods learn representations on the *hypersphere*, their relevance to the spherical variational inference [7] has not been discussed.

Multimodal variational autoencoder [24, 45, 39, 40] are trained to infer latent variables from *multiple observations*<sup>1</sup> from different modals. The latent variable distribution of multimodal variational inference is often assumed as the *product of experts* or the *mixture of experts* of unimodal distributions [24, 45, 39]. Sutter et al. [40] also clarified the connection between them and generalized them as mixture-of-products-of-experts-VAE. Multimodal variational inference seems to be highly related to SSL utilizing *multiview inputs*. However, their relation has been unclear.

### 2.3 Uncertainty-aware methods

Uncertainty-aware methods [9, 19, 20] have been proposed to solve the problem that data with high uncertainty will hinder learning. Kendall and Gal [19] proposed the method that estimates data uncertainty in regression and classification tasks by assuming that outputs follow a normal distribution. Scott et al. [38] proposed a stochastic spherical loss for classification tasks based on the von Mises–Fisher distributions. Uncertainty-aware methods have been proposed for other tasks, such as human pose estimation [36, 33, 12], optical flow estimation [18], object detection [17, 14], and reinforcement learning [26, 32, 13].

In self-supervised learning, some methods that incorporate uncertainty [37, 48, 34, 43] have been investigated. Several studies [37, 48, 34] have proposed methods for SSL to estimate uncertainty helpful in learning specific tasks such as depth estimation, image recovery, and multiview stereo, which are different from learning representations that incorporate uncertainty. Wang et al. [43] proposed uncertainty-aware self-supervised representation learning for three dimensional (3D) object tracking. The method learns representations by contrastive learning [3, 15] and estimates uncertainty by comparing the Mahalanobis distances [27] of positive and negative pairs. This method requires negative pairs and object tracking task properties for uncertainty estimation. Therefore, general uncertainty-aware non-contrastive self-supervised representation learning has not been proposed.

## 3 Preliminary

This section briefly reviews the theories of non-contrastive SSL and variational inference.

### 3.1 Non-contrastive self-supervised learning

The loss function of non-contrastive SSL, such as BYOL and SimSiam is generally described as follows:

$$\mathcal{L}_{\text{SSL}} := -g(x_1)^\top f(x_2) - g(x_2)^\top f(x_1), \quad (1)$$

where  $x_{1,2}$  are two augmented views of a single image, while  $g$  and  $f$  are different encoders. This loss function maximizes the cosine similarity of features from different views. The two encoders are referred to as *online* and *target* networks respectively. The online network is trained to minimize the loss. The target network is not trained by back-propagation, and it is updated by directly copying weights of the online network (e.g., SimSiam) or slowly following the online network through an exponential moving average (e.g., BYOL).

### 3.2 Multimodal variational inference

Fig. 2 shows a graphical model for multimodal variational inference, where  $\mathbb{X} = \{x_i\}_{i=1}^M$  is a set of multimodal observations  $x_i$ ,  $z$  is a latent variable of the observations, and  $M$  is the number of modalities, which correspond to the types of data augmentation in this paper. In the context of SSL,  $\mathbb{X}$  can be regarded as augmented images from stochastic generative processes. The objective of the variational inference problem is to find a parameterized variational distribution  $q_\phi(z|\mathbb{X})$  that minimizes the Kullback–Leibler divergence between the posterior  $p(z|\mathbb{X})$ :

$$\mathcal{L}_{\text{KL}} := D_{\text{KL}}(q_\phi(z|\mathbb{X})||p(z|\mathbb{X})). \quad (2)$$

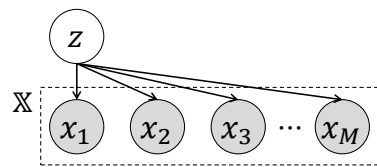


**Figure 2:** Graphical model for representing data augmentation as a multimodal probabilistic generative model.

<sup>1</sup>We treat multiple observations as *multiview* and *multimodal*.

Generally, this optimization problem is solved using a variational autoencoding scheme, involving a parameterized generative model  $p_\theta(\mathbb{X}|z)$ . The posterior is formulated with the generative model and Bayes' theorem as follows:

$$p(z|\mathbb{X}) \simeq p_\theta(\mathbb{X}|z)p(z)/p(\mathbb{X}). \quad (3)$$

Substituting Eq. (3) in Eq. (2), we obtain the well-known evidence lower bound (ELBO) objective:

$$\mathcal{L}_{\text{ELBO}} := -\mathbb{E}_{q_\phi}[\log p_\theta(\mathbb{X}|z)] + D_{\text{KL}}(q_\phi(z|\mathbb{X})||p(z)) \propto \mathcal{L}_{\text{KL}}. \quad (4)$$

## 4 Self-supervised learning as inference

In this section, we show a connection between non-contrastive self-supervised learning and multi-modal variational inference. Let us recall Eq. (2). Instead of introducing a parametrized generative model  $p_\theta(x|z)$  via Eq. (3), we directly introduce a different parametrized posterior  $p_\psi(z|\mathbb{X})$ <sup>2</sup>. Eq. (2) can be reformulated as follows:

$$\mathcal{L}_{\text{KL}} = -\mathbb{E}_{q_\phi}[\log p_\psi(z|\mathbb{X})] + \mathbb{E}_{q_\phi}[\log q_\phi(z|\mathbb{X})]. \quad (5)$$

It should be noted that this is a loss function that generalizes the non-contrastive SSL loss of Eq. (1). The remaining section demonstrates that the non-contrastive can be recovered from Eq. (5) by defining  $p_\psi$  and  $q_\phi$  as hyperspherical distributions.

We suppose that the posterior takes the form of *product of experts* comprising von-Mises-Fisher (vMF) distributions:

$$p_\psi(z|\mathbb{X}) := \prod_{i=1}^M \text{vMF}(z; g_\psi(x_i), \kappa), \quad (6)$$

$$\text{vMF}(z; \mu, \kappa) := C(\kappa) \exp(\kappa \mu^\top z). \quad (7)$$

where, encoder  $g_\psi$  embeds observations into a hyperspherical latent space, parameters  $\mu$  and  $\kappa$  are the mean direction and concentration parameter, and  $C(\kappa)$  is a normalization constant defined with the modified Bessel function. We define the variational model as a *mixture of experts* of deterministic distributions:

$$q_\phi(z|\mathbb{X}) := \frac{1}{M} \sum_{j=1}^M \delta(z - f_\phi(x_j)). \quad (8)$$

Under the definition of  $q_\phi$ , the second term in Eq. (5) is constant. Consequently, we derive the objective function, which is similar to that of Eq. (1):

$$\mathcal{L}_{\text{KL}} \propto -\sum_{i=1}^M \sum_{j=1}^M g_\psi^\top(x_i) f_\phi(x_j) \quad (9)$$

where, we used the relations of  $\mathbb{E}_{q_\phi}[\cdot] = \sum_i \mathbb{E}_{\delta(z-f_\phi(x_i))}[\cdot]$  and  $\mathbb{E}_{\delta(z-f_\phi(x_i))}[\log p_\psi(z|\mathbb{X})] = \log p_\psi(f_\phi(x_i)|\mathbb{X})$ . In Eq. (9), cross-modal comparison is naturally appeared. Comparisons of same modals (i.e.,  $i = j$ ) provide less effective information for training. thus we can practically ignore those terms. In this formulation,  $\kappa$  is regarded as a constant; hence computation of  $C(\kappa)$  is unnecessary.

## 5 Variational inference SimSiam

In this section, we introduce a novel uncertainty-aware SSL method by exploiting the previously derived principle of *SSL as inference*. The previous derivation assumes that the concentration parameter  $\kappa$  is constant, ignoring the uncertainty in the representations. We relax this assumption, and allow  $\kappa$  to be estimated by the encoder, along with  $\mu$ ; i.e.,  $g_\psi : x_i \rightarrow (\mu_i, \kappa_i)$ . Additionally, we replace the vMF distribution with another spherical distribution, the power spherical (PS) distribution [8], because

---

<sup>2</sup>Note that the relationship between the parametrized generative model  $p_\theta(\mathbb{X}|z)$  in usual variational inference and the proposed parametrized model  $p_\psi(z|\mathbb{X})$  is:  $p_\theta(\mathbb{X}|z) = p_\psi(z|\mathbb{X})p(\mathbb{X})/p(z)$ .

---

**Algorithm 1** Pseudocode, PyTorch-like

---

```

# f: ResNet-backbone + Projector
# h: Predictor

class PSd(Distribution):
    # Definition of power spherical distribution.
    # Code is taken from:
    # github.com/nicola-decao/power_spherical
    def __init__(self, mu, kappa):
        ...

    for x in loader: # Load a minibatch x
        x1, x2 = aug(x), aug(x) # Apply augmentation
        z1, z2 = f(x1), f(x2) # Project

        # Predict
        (mu1, kappa1), (mu2, kappa2) = h(z1), h(z2)
        p1, p2 = PSd(mu1, kappa1), PSd(mu2, kappa2)

        # Stop gradient & compute loss
        z1, z2 = z1.detach(), z2.detach()
        L = - p1.log_prob(z2) - p2.log_prob(z1)
        L.mean().backward() # Back-prop.
        update(f, h) # SGD update

```

---

computing gradients through the modified Bessel function in the vMF distribution is computationally expensive and unstable [8]. The modified posterior is defined as:

$$p_\psi(z|\mathbb{X}) := \prod_{i=1}^M \text{PS}(z; \mu_i, \kappa_i), \quad (10)$$

$$\text{PS}(z; \mu, \kappa) := C(\kappa)(1 + \mu^\top z)^\kappa. \quad (11)$$

The normalization constant of PS distribution  $C(\kappa)$  is defined with the beta distribution, which can be efficiently computed by general deep learning frameworks. Substituting Eqs.(8) and (11) into Eq. (5) yields:

$$\mathcal{L}_{\text{KL}} = - \sum_{i=1}^M \sum_{j=1}^M \left( \log C(\kappa_i) - \kappa_i \log (1 + \mu_i^\top f_\phi(x_j)) \right). \quad (12)$$

Like Eqs. (1) and (9), this loss is to maximize the cosine similarity of features from different modals, but the similarity term is weighted by  $\kappa$ . Figure 3 visualizes the loss function with varying cosine similarities and  $\kappa$ s, where we can observe that a high uncertainty (or low  $\kappa$ ) makes the loss values almost constant to reduce the effect of similarity mismatch.

We propose a novel method referred to as variational inference SimSiam (VI-SimSiam) by modifying SimSiam to optimize Eq. (12) instead of Eq. (1). The architecture and pseudocode are shown in Fig. 1 and Alg. 1, respectively, where the number of modality  $M$  is set to be  $M = 2$ . In our method, we define  $g_\psi$  and  $f_\phi$  as online and target networks with the same structures are as in SimSiam [4];  $g_\psi$  is defined as  $g_\psi = h_\psi \circ f_\phi$ , where  $h_\psi$  is a predictor network [11, 4]. A major difference from SimSiam is that  $g_\psi$  predicts the concentration  $\kappa$ .

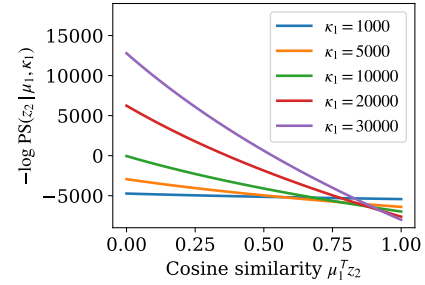


**Figure 3:** Visualization of a part of the newly derived loss function Eq. (12), with varying cosine similarities and  $\kappa$ s.

Dataset	SimSiam		VI-SimSiam		mean of $\kappa$	std of $\kappa$
	Top-1	Top-5	Top-1	Top-5		
ImageNette	88.2	98.2	<b>90.7</b>	<b>99.4</b>	11527	7505
ImageWoof	72.4	97.5	<b>78.4</b>	<b>98.1</b>	8148	4908
Flowers	<b>24.6</b>	<b>51.5</b>	19.7	43.9	170	132
Food	<b>69.7</b>	<b>90.5</b>	62.1	85.6	7478	16101
DTD	<b>26.6</b>	<b>54.0</b>	24.9	53.4	3522	889
Aircraft	7.0	20.3	<b>7.9</b>	<b>24.7</b>	8046	3900
SUN397	34.2	68.4	<b>39.8</b>	<b>74.1</b>	5535	2110
Pet	24.0	60.3	<b>30.6</b>	<b>68.4</b>	3672	1460
Cars	12.7	33.2	<b>14.9</b>	<b>37.2</b>	13087	7370

**Table 1:** Top-1 or 5 accuracies in the linear evaluation, mean and std of  $\kappa$  of train split.

## 6 Experiments

We evaluate the performance of VI-SimSiam and compared it to that of SimSiam. First, we perform a linear evaluation of these methods on nine classification datasets (ImageNette [10], ImageWoof [10], Flowers [30], Food [1], DTD [6], Aircraft [28], SUN397 [47, 46], Pet [35], and Cars [23]). This protocol is designed to evaluate pretrained features by freezing the backbone weights and training only a linear classifier. We also evaluate our method under a more realistic experimental setting, semi-supervised learning with a 1% or 10% label. Each experiment needs single NVIDIA GeForce RTX 3070.

### 6.1 Linear evaluation

We conducted self-supervised pretraining with a dataset without labels to learn image representations using SimSiam and VI-SimSiam at 100 epochs. Then, we train a linear classifier on frozen representations on the training set of the dataset with the label. Finally, we evaluate it in the test set of the dataset. We report the implementation details in Appendix 9.1. We use top-1 and top-5 accuracies as evaluation metrics. We use classification datasets. In some datasets (e.g., ImageNette, ImageWoof, Food, Cars and Pet), the datasets have only split into two parts (e.g., training and validation, training and test). When we use them, we set about 20% of the training split as a local validation split for tuning parameters. Table 1 presents top-1 and top-5 accuracies on the test set. VI-SimSiam outperformed SimSiam on six of nine data set.

Table 1 also presents the mean and std of  $\kappa$  of train split. We also show the boxplot of  $\kappa$  of train split in Fig. 4. Eight views generated per image are by random augmentation, and the  $\kappa$  of each view is estimated. Flowers and DTD show no improvement in accuracy with VI-SimSiam, and the variance of  $\kappa$  is smaller than that of other datasets. In VI-SimSiam,  $\kappa$  related to uncertainty adjusts the loss value; thus, a dataset with a small variance of  $\kappa$  may have a lower learning effect from incorporating uncertainty. Food has many outliers of  $\kappa$ . It could be overfitting because this result indicates that some latent variables are estimated to have extremely low uncertainty.

### 6.2 Semi-supervised learning

We evaluate the performance of the proposed method in a more realistic experimental setting, semi-supervised learning. Given the high cost of labeling and the situation where only some data are labeled, we use labels for only 1% or 10% of the total ImageNette and ImageWoof. After pretraining networks without labels at 100 epochs, we finetune the entire networks at 200 epochs with labeled data, with a batch size of 256. Table 2 presents the top-1 accuracy of each setting. Consequently, we obtained that VI-SimSiam consistently outperformed SimSiam in all settings.

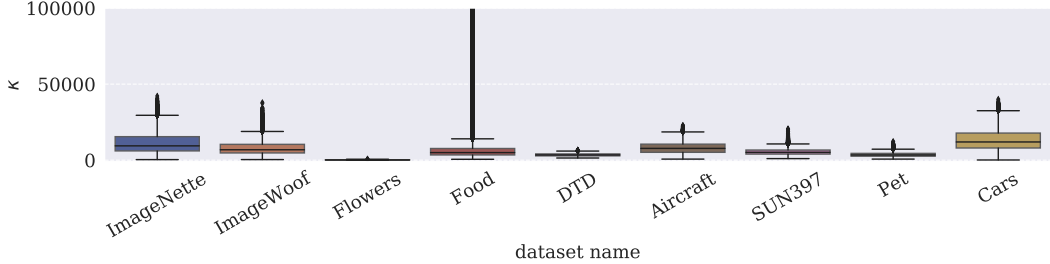


**Figure 4:** Boxplot of the concentration  $\kappa$  of each dataset’s training split. Flower and DTD have less variance than other datasets; thus, they may have a smaller learning effect from incorporating uncertainty. Food has many outliers, and some of the data may be overfitted.

Method	ImageNette		ImageWoof	
	1%	10%	1%	10%
scratch	30.5	61.1	19.6	41.7
SimSiam [4]	64.2	85.0	39.6	69.0
VI-SimSiam	<b>74.5</b>	<b>87.7</b>	<b>48.3</b>	<b>75.9</b>

**Table 2:** Top-1 accuracies under semi-supervised learning.

### 6.3 Visualization

We visualize the image features converted to 2D in t-SNE in the validation set of ImageNette and ImageWoof in Fig. 5. Each point denotes the feature of an image. Different colors denote different classes. In SimSiam, several classes of samples are plotted in the same area, and it seems that classification is not as easy as in VI-SimSiam, especially in ImageWoof. Fig. 6 also shows the boxplot of  $\kappa$ s of each class. Classes with relatively large  $\kappa$  in the dataset appear to have many samples mapped on a close space. (e.g., *Samoyed*, *Old English sheepdog*) Meanwhile, classes with relatively small  $\kappa$  appear to have some samples mapped close to the samples of other classes (e.g., *Australian terrier*, *Border terrier*, and *dingo*).

## 7 Discussion

**Relation to input images;** We conduct a qualitative evaluation of uncertainty estimation by comparing an input image to the predicted concentration  $\kappa$ , a parameter related to the uncertainty with ImegeNette dataset. Fig. 7a shows input images and the histogram of predicted  $\kappa$ . The input image is the original image resized to  $256 \times 256$  and cropped in the center to  $224 \times 224$ . When  $\kappa$  is predicted to be low, i.e., the uncertainty of the latent variable is predicted to be high, there are few noticeable features in the input images. In contrast, when  $\kappa$  is predicted to be high, i.e., the uncertainty of the latent variable is predicted to be low, there are noticeable features in the input images, e.g., various colors and edges. This result shows that the proposed method can learn the uncertainty of the latent variable.

**Relation to downstream task;** We investigate the effects of uncertainty on a downstream image classification task with ImageNette dataset. We compared the uncertainty between images for which the correct and incorrect labels are estimated. Fig. 7b shows boxplots of  $\kappa$ s for samples for which the estimated labels are correct and incorrect. Consequently, we obtained that the  $\kappa$  of image features in which the incorrect label is estimated are lower than those for which the correct label is estimated ( $p < 0.01$ ). This result shows that the uncertainty is related to the difficulty of classification.

**Relation to image augmentation;** We investigate how image augmentations affect uncertainty. We use the validation dataset of ImageNette. We also prepare image augmentations for *blur*, *color jitter*, *flip*, *grayscale* and *random crop*. The random crop scale for *random crop* is set from 0.05 to 1.0. For each image, we performed five augmentations and calculated the average of concentration  $\kappa$  estimated by the pretrained model for each augmentation. Fig 8a shows the boxplot of concentration  $\kappa$  for each augmentation. The variance of the  $\kappa$  of *random crop* is larger than that of other augmentations.

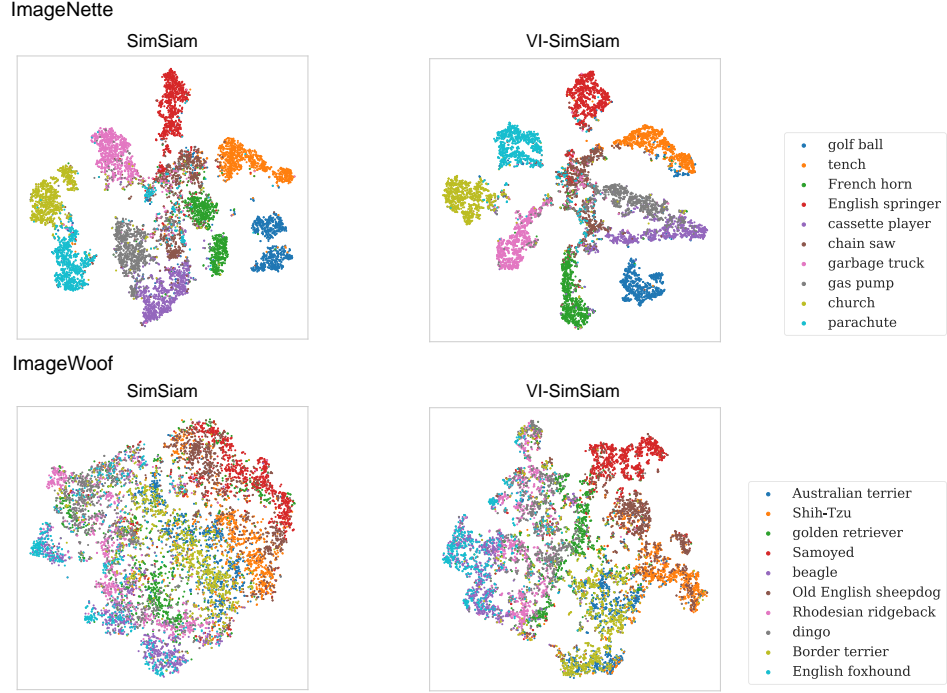


**Figure 5:** Visualization of image features converted to 2D in t-SNE in validation of ImageWoof. Each point denotes the feature of an image. Different colors denote different classes.

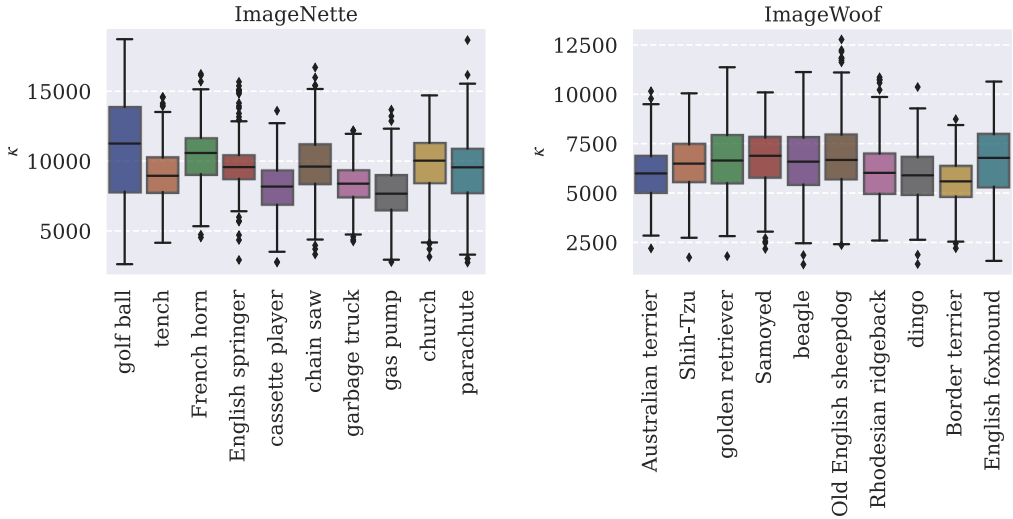


**Figure 6:** Boxplot of the  $\kappa$ s of each class of ImageNette and ImageWoof.

Fig 8b shows the examples of images that applied *random crop*. The *random crop* can completely exclude objects important for latent variable estimation from the input view, as in the examples in the right column. It can also generate a view with only important objects for latent variable estimation, as in the examples in the center column. These phenomena seem to be the reason why the variance of  $\kappa$  is larger at the *random crop*.

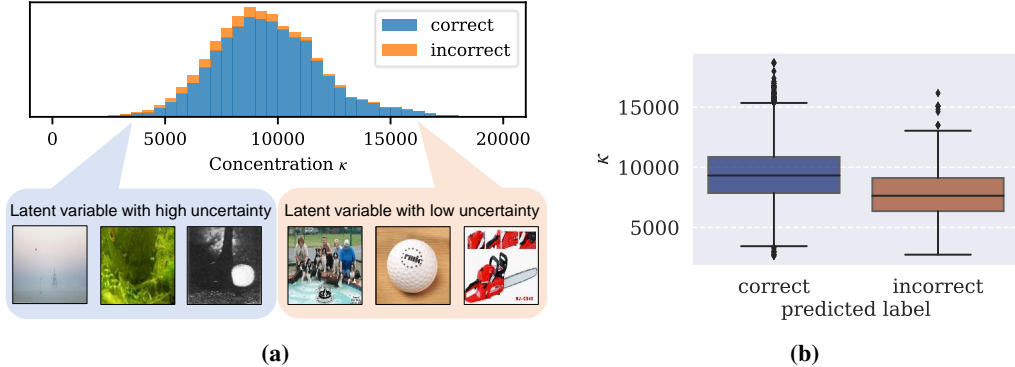


**Figure 7:** (a) Histogram of the estimated concentration  $\kappa$  and selected input images. Correct and incorrect samples are shown in blue and orange for frequencies, respectively. Latent variables of these images have high and low uncertainty. Images with low uncertainty in latent variables appear to have less salient features than that of the others. (b) Boxplot of the estimated concentration  $\kappa$ s and estimated labels correctness. This result shows that uncertainty of image features affects the difficulty of classification.

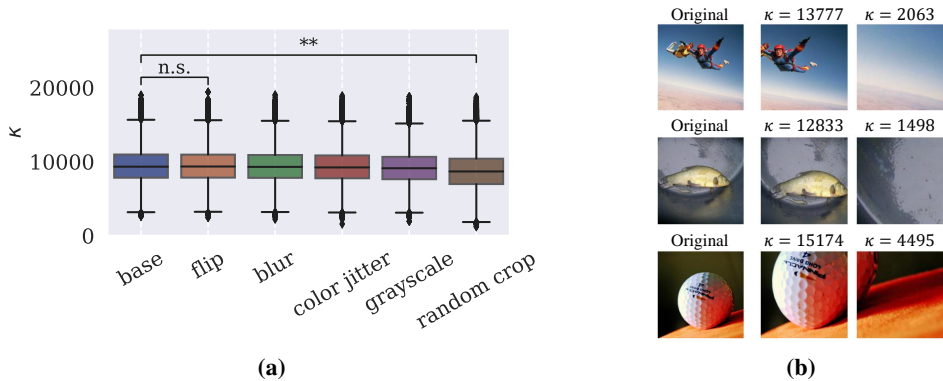


**Figure 8:** (a) Boxplot of the  $\kappa$ s of each augmentation. *base* means that no augmentations are applied. Symbols ‘\*\*’ and ‘n.s.’ respectively mean  $p < 0.01$  and  $p \geq 0.01$  in Welch’s t-test. (b) Example of cropped images and  $\kappa$ s; the images on the left are original images. the images at the center and right are cropped images.

## 8 Conclusion

In this paper, we clarify the theoretical relationship between variational inference and non-contrastive self-supervised learning and propose variational inference SimSiam (VI-SimSiam), which can model the uncertainty of the latent variable. We demonstrated the effectiveness of the proposed VI-SimSiam by evaluating it with image classification task using pretrained image features.

Various experiments demonstrated the effectiveness of the proposed method; however it is possible that future efforts will further improve its performance. As mentioned in Sec. 6.1, the current method can cause overfitting in some datasets. Our method would be more effective if a solution to this issue (e.g., early stopping) could be proposed.

## References

- [1] Lukas Bossard, Matthieu Guillaumin, and Luc Van Gool. Food-101 – mining discriminative components with random forests. In *ECCV*, 2014.
- [2] Mathilde Caron, Ishan Misra, Julien Mairal, Priya Goyal, Piotr Bojanowski, and Armand Joulin. Unsupervised learning of visual features by contrasting cluster assignments. *NeurIPS*, 2020.
- [3] Ting Chen, Simon Kornblith, Mohammad Norouzi, and Geoffrey Hinton. A simple framework for contrastive learning of visual representations. In *ICML*, 2020.

- [4] Xinlei Chen and Kaiming He. Exploring simple siamese representation learning. In *CVPR*, 2021.
- [5] Xinlei Chen, Saining Xie, and Kaiming He. An empirical study of training self-supervised vision transformers. In *ICCV*, 2021.
- [6] M. Cimpoi, S. Maji, I. Kokkinos, S. Mohamed, , and A. Vedaldi. Describing textures in the wild. In *CVPR*, 2014.
- [7] Tim R Davidson, Luca Falorsi, Nicola De Cao, Thomas Kipf, and Jakub M Tomczak. Hyperspherical variational auto-encoders. In *UAI*, 2018.
- [8] Nicola De Cao and Wilker Aziz. The power spherical distribution. *ICML, INNF+*, 2020.
- [9] Armen Der Kiureghian and Ove Ditlevsen. Aleatory or epistemic? does it matter? *Structural safety*, 2009.
- [10] fast.ai. Imagenette: A smaller subset of 10 easily classified classes from imagenet. <https://github.com/fastai/imagenette>, 2020.
- [11] Jean-Bastien Grill, Florian Strub, Florent Altché, Corentin Tallec, Pierre Richemond, Elena Buchatskaya, Carl Doersch, Bernardo Avila Pires, Zhaohan Guo, Mohammad Gheshlaghi Azar, et al. Bootstrap your own latent-a new approach to self-supervised learning. *NeurIPS*, 2020.
- [12] Nitesh B Gundavarapu, Divyansh Srivastava, Rahul Mitra, Abhishek Sharma, and Arjun Jain. Structured aleatoric uncertainty in human pose estimation. In *CVPRW*, 2019.
- [13] Wei Guo, Marc Brittain, and Peng Wei. Safety enhancement for deep reinforcement learning in autonomous separation assurance. In *ITSC*, 2021.
- [14] David Hall, Feras Dayoub, John Skinner, Haoyang Zhang, Dimity Miller, Peter Corke, Gustavo Carneiro, Anelia Angelova, and Niko Sünderhauf. Probabilistic object detection: Definition and evaluation. In *WACV*, 2020.
- [15] Kaiming He, Haoqi Fan, Yuxin Wu, Saining Xie, and Ross Girshick. Momentum contrast for unsupervised visual representation learning. In *CVPR*, 2020.
- [16] Kaiming He, Xiangyu Zhang, Shaoqing Ren, and Jian Sun. Deep residual learning for image recognition. In *CVPR*, 2016.
- [17] Yihui He, Chenchen Zhu, Jianren Wang, Marios Savvides, and Xiangyu Zhang. Bounding box regression with uncertainty for accurate object detection. In *CVPR*, 2019.
- [18] Eddy Ilg, Ozgun Cicek, Silvio Galesso, Aaron Klein, Osama Makansi, Frank Hutter, and Thomas Brox. Uncertainty estimates and multi-hypotheses networks for optical flow. In *ECCV*, 2018.
- [19] Alex Kendall and Yarin Gal. What uncertainties do we need in bayesian deep learning for computer vision? In *NeurIPS*, 2017.
- [20] Alex Kendall, Yarin Gal, and Roberto Cipolla. Multi-task learning using uncertainty to weigh losses for scene geometry and semantics. In *CVPR*, 2018.
- [21] Diederik P Kingma and Max Welling. Auto-encoding variational Bayes. *arXiv preprint arXiv:1312.6114*, 2013.
- [22] Nikos Komodakis and Spyros Gidaris. Unsupervised representation learning by predicting image rotations. In *ICLR*, 2018.
- [23] Jonathan Krause, Michael Stark, Jia Deng, and Li Fei-Fei. 3d object representations for fine-grained categorization. In *ICCVW*, 2013.
- [24] Richard Kurle, Stephan Günemann, and Patrick Van der Smagt. Multi-source neural variational inference. In *AAAI*, 2019.
- [25] Xiao Liu, Fanjin Zhang, Zhenyu Hou, Li Mian, Zhaoyu Wang, Jing Zhang, and Jie Tang. Self-supervised learning: Generative or contrastive. *TKDE*, 2021.
- [26] Björn Lütjens, Michael Everett, and Jonathan P How. Safe reinforcement learning with model uncertainty estimates. In *ICRA*, 2019.
- [27] Prasanta Chandra Mahalanobis. On the generalized distance in statistics. National Institute of Science of India, 1936.
- [28] Subhransu Maji, Esa Rahtu, Juho Kannala, Matthew Blaschko, and Andrea Vedaldi. Fine-grained visual classification of aircraft. *arXiv preprint arXiv:1306.5151*, 2013.
- [29] Alejandro Newell and Jia Deng. How useful is self-supervised pretraining for visual tasks? In *CVPR*, 2020.
- [30] M-E Nilsback and Andrew Zisserman. A visual vocabulary for flower classification. In *CVPR*, 2006.
- [31] Mehdi Noroozi and Paolo Favaro. Unsupervised learning of visual representations by solving jigsaw puzzles. In *ECCV*, 2016.

- [32] Masashi Okada, Norio Kosaka, and Tadahiro Taniguchi. Planet of the bayesians: Reconsidering and improving deep planning network by incorporating bayesian inference. In *IROS*, 2020.
- [33] Masashi Okada, Shinji Takenaka, and Tadahiro Taniguchi. Multi-person pose tracking using sequential monte carlo with probabilistic neural pose predictor. In *ICRA*, 2020.
- [34] Tongyao Pang, Yuhui Quan, and Hui Ji. Self-supervised bayesian deep learning for image recovery with applications to compressive sensing. In *ECCV*, 2020.
- [35] Omkar M Parkhi, Andrea Vedaldi, Andrew Zisserman, and CV Jawahar. Cats and dogs. In *CVPR*, 2012.
- [36] Ilia Petrov, Vlad Shakhuro, and Anton Konushin. Deep probabilistic human pose estimation. *IET Computer Vision*, 2018.
- [37] Matteo Poggi, Filippo Aleotti, Fabio Tosi, and Stefano Mattoccia. On the uncertainty of self-supervised monocular depth estimation. In *CVPR*, 2020.
- [38] Tyler R Scott, Andrew C Gallagher, and Michael C Mozer. von mises-fisher loss: An exploration of embedding geometries for supervised learning. In *ICCV*, 2021.
- [39] Yuge Shi, Brooks Paige, Philip Torr, et al. Variational mixture-of-experts autoencoders for multi-modal deep generative models. *NeurIPS*, 2019.
- [40] Thomas M. Sutter, Imant Daunhawer, and Julia E Vogt. Generalized multimodal ELBO. In *ICLR*, 2021.
- [41] Yuandong Tian, Xinlei Chen, and Surya Ganguli. Understanding self-supervised learning dynamics without contrastive pairs. In *ICML*, 2021.
- [42] Jakub Tomczak and Max Welling. Vae with a vampprior. In *AISTATS*, 2018.
- [43] Jianren Wang, Siddharth Ancha, Yi-Ting Chen, and David Held. Uncertainty-aware self-supervised 3d data association. In *IROS*, 2020.
- [44] Tongzhou Wang and Phillip Isola. Understanding contrastive representation learning through alignment and uniformity on the hypersphere. In *ICML*, 2020.
- [45] Mike Wu and Noah Goodman. Multimodal generative models for scalable weakly-supervised learning. *NeurIPS*, 2018.
- [46] Jianxiong Xiao, Krista A Ehinger, James Hays, Antonio Torralba, and Aude Oliva. Sun database: Exploring a large collection of scene categories. *IJCV*, 2016.
- [47] Jianxiong Xiao, James Hays, Krista A Ehinger, Aude Oliva, and Antonio Torralba. Sun database: Large-scale scene recognition from abbey to zoo. In *CVPR*, 2010.
- [48] Hongbin Xu, Zhipeng Zhou, Yali Wang, Wenxiong Kang, Baigui Sun, Hao Li, and Yu Qiao. Digging into uncertainty in self-supervised multi-view stereo. In *ICCV*, 2021.
- [49] Yang You, Igor Gitman, and Boris Ginsburg. Large batch training of convolutional networks. *arXiv preprint arXiv:1708.03888*, 2017.
- [50] Jure Zbontar, Li Jing, Ishan Misra, Yann LeCun, and Stéphane Deny. Barlow twins: Self-supervised learning via redundancy reduction. In *ICML*, 2021.

## 9 Appendix

### 9.1 Implementation details

**Experimental settings for networks;** VI-SimSiam’s architecture of the encoder  $f$  and the predictor  $h$  is almost identical to that of SimSiam. Unlike SimSiam’s setting, we use Resnet18 [16] as a backbone network of the encoder  $f$ . We also add one dimension of the output layer of the predictor  $h$  to predict  $\kappa$ .

**Experimental Settings for pretraining;** We use momentum-SGD for pretraining. The learning rate is 1e-3. The weight decay is 1e-4, and the SGD momentum is 0.9. The learning rate has a cosine decay schedule. The batch size is 64. We perform 100-epoch pretraining. We incorporate multi-crop [2] into augmentation. Multi crop uses two types of views for training: standard and small resolution views. Standard resolution views are generated by the same augmentation setting as SimSiam. In SimSiam, there are five different types of augmentation (*blur, color jitter, flip, grayscale* and *random crop*), with each augmentation applied and its strength randomly determined. Fig 9 shows the examples of augmented views. Low resolution views are generated by the augmentation setting of SimSiam with modified random crop and resize parameters. In the augmentation setting of low resolution views, the random crop scale is from 0.05 to 0.2, and the size is  $96 \times 96$ . We use two standard resolution views and six low resolution views per image in each experiment.

**Experimental settings for linear-evaluation;** We use LARS [49] as an optimizer for the linear-evaluation. The learning rate is 1.6. The weight decay is 0.0, and the SGD momentum is 0.9. The batch size is 512. The image augmentation and preprocessing are referred to as that of SimSiam. We trained 200 epochs and tested the model with the highest Top-1 accuracy for the validation set.

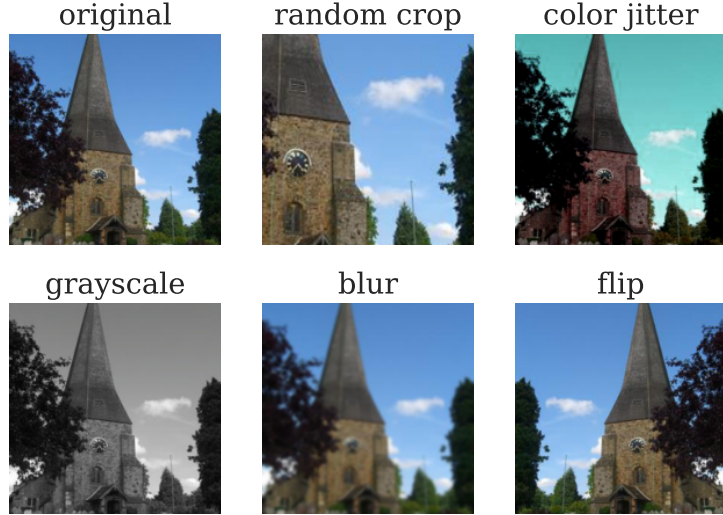


**Figure 9:** The examples of augmented images.